Letter

Improved Stability of Inverted and Flexible Perovskite Solar Cells with Carbon Electrode

Vivek Babu, Rosinda Fuentes Pineda, Taimoor Ahmad, Agustin O. Alvarez, Luigi Angelo Castriotta, Aldo Di Carlo, Francisco Fabregat-Santiago, and Konrad Wojciechowski*

Cite This: *ACS Appl. Energy Mater.* 2020, 3, 5126–5134

Read Online

ACCESS | Metrics & More | Article Recommendations | Supporting Information

ABSTRACT: We demonstrate highly efficient, stable, and flexible perovskite solar cells of large areas, utilizing a carbon back-contact electrode in a p−i−n cell configuration. We enabled good electronic contact at the interface with carbon by inserting an ultrathin buffer layer before the carbon coating. Solar cells of such structure reach a power conversion efficiency of 15.18% on PET foil (device area of 1 cm^2). We performed impedance spectroscopy and transient decay measurements to understand the electron transport characteristics. Furthermore, we demonstrate excellent operational (maximum power point) and thermal (85 °C) stability of these devices over 1000 h of aging.
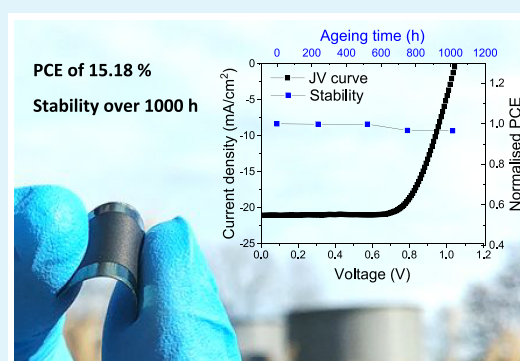
Perovskite solar cells (PSCs) over the years became a frontrunner of emerging photovoltaic technologies and attracted a lot of attention from researchers across various disciplines.[1] The reported power conversion efficiencies (PCEs) underwent a steep rise, reaching a certified value of 25.2% in 2019.[2] Such a prolific pace of technological advancement can be linked with extraordinary optoelectronic properties of this class of semiconductors, including high absorptivity, large carrier diffusion lengths, mixed ionic/ electronic conductivity, and peculiar defect chemistry taking place in thin films of these materials.[3−7] Additionally, perovskite polycrystalline films can be solution-processed with a low temperature annealing step, which opens attractive new value propositions for industrial applications. There is an increasing interest in the thin-film PV technologies capable of offering new, disrupting solutions, such as simple and low cost manufacturing, high mechanical flexibility, and high specific power (lightweight with high power output).[8] However, the long-term stability remains one of the major concerns for the large-scale utilization of the perovskite technology.[9,10] Recently, a consensus on the procedures for testing the PSC reliability between multiple research groups working on this technology was reported.[11]

Metallic layers, such as gold or silver, are typically used as back-contact electrode materials in the state-of-the-art perovskite solar cells. Domanski et al. found that a considerable amount of gold from the back-contact can diffuse across the hole transport layer (HTL) into the perovskite material, resulting in a dramatic loss of device performance.[12] In another work, Li et al. showed the direct evidence of the PSC degradation due to the ion migration from the perovskite layer to the silver electrode.[13] This results in the formation of an insulating silver halide, which eventually hampers the charge extraction properties.[13,14] Moreover, gold and silver are expensive for mass production and require highly energy-demanding and vacuum-based deposition steps.

Carbon was demonstrated as an effective back-contact electrode material for the perovskite solar cells, a possible alternative to metallic layers.[15−18] Carbon pastes are typically composed of graphite flakes and carbon black powder. The blends of these materials display a relatively deep work function (ca. 5.0 eV); hence, they were predominantly used for hole collection in perovskite solar cells and so were applied as a back-contact in the standard PSC configuration (mesoscopic and planar n−i−p architecture). The first utilization of the carbon electrode in a perovskite PV stack was done by Ku et al. in a hole transporter-free, mesoscopic device structure, yielding a PCE of 6.6%.[19] Since then, the HTM-free architectures became quite popular; they are typically composed of multiple metal oxides (compact TiO$_2$, mesoporous TiO$_2$, and insulating
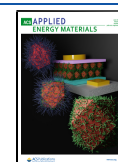
mesoporous spacer, like ZrO_2) sequentially deposited on FTO glass. Subsequently, the carbon layer is coated on top, and the whole stack is infiltrated with a perovskite precursor solution. Perovskite material crystallizes within the pores of the mesoscopic oxides. Grancini et al. reported the HTM-free, carbon-based modules with the impressive operational stability, obtaining 10 000 h without any loss in performance.[20] However, these structures typically require a high temperature (400 °C) sintering step for the preparation of metal oxide and carbon layers. An important development was achieved by the demonstration of carbon pastes processable at low temperatures (below 100 °C), which enabled the use of flexible, polymeric substrates.[21] Another shortfall of the hole transporter-free PSC architecture is poor carrier selectivity at the carbon interface, which leads to a significant charge recombination and in turn poor device performance. It seems advantageous to have an additional charge selective layer between the perovskite and carbon electrode, which could reduce recombination losses and improve carrier selectivity at that contact. Recently, Chu et al. fabricated carbon-based planar PSC (n−i−p configuration) using graphene-doped P3HT as an HTL, delivering 18.1% efficiency for glass, and 12.4% for a flexible substrate, which was combined with improved ambient stability.[22] In addition to the stability aspects, carbon is cheap and abundant; these are are very attractive features from an industrial point of view. As mentioned earlier, all the efficient perovskite solar cells with a solution-processed carbon electrode reported to date were fabricated in the device architectures where holes were extracted at the carbon contact.

A so-called "inverted" perovskite solar cell architecture (p−i−n configuration) has attracted sizable interest over the years, mainly due to its ease of fabrication (facile solution-based processing without high temperature annealing steps) and a large selection of cost-effective charge transport materials, many of them working effectively without the need of doping.[23,24] Historically, p−i−n PSCs lagged behind a standard cell configuration in reported efficiencies, but recently, multiple examples of inverted devices over 20% PCE were demonstrated, with a record performance as high as 22.3%, and over 16% at the module level.[25,26] However, the best reported p−i−n devices use metallic layers for the back-contact electrode (thermally evaporated silver or copper), which can pose limitations to the long-term stability, especially at elevated temperatures, as discussed above.

In this work, we are demonstrating an effective use of carbon as a back-contact electrode material in planar heterojunction perovskite solar cells of p−i−n architecture (electron collection at the back-contact). This is achieved by introducing an ultrathin buffer layer of chromium (Cr) between the ETL and carbon electrode, which enables Ohmic contact between these layers and effective collection of electrons. We selected a carbon paste processable at low temperatures to be able to apply it on top of perovskite material and to use plastic foil substrates. We fabricated large-area (1 cm^2) flexible perovskite solar cells, reaching the PCE of 15.18%. To the best of our knowledge, this is the highest reported efficiency for a flexible perovskite solar cell embedding a carbon back-contact electrode. We applied impedance spectroscopy and transient photocurrent and photovoltage decay measurements to study the electron extraction through the Cr/C interface. In addition to p−i−n structures, we are also demonstrating that Cr can be used as a buffer layer in the n−i−p PSC configuration, yielding

the PCE of 12.06%. Furthermore, we are showing stability results from the maximum power point and thermal (85 °C) aging tests, demonstrating excellent reliability of carbon-based devices.

We deposited carbon films with a blade-coating technique using a commercial carbon paste supplied by Dyenamo. We varied processing parameters to optimize thickness and annealing conditions of the coated layers. We obtained the film thickness of 20 μm (recommended by the supplier) by adjusting a gap between the blade and the substrate (50 μm) and the coating speed (5 mm/s), as shown in Figure S1a. For the curing step of deposited carbon films, we applied a gas blowing method using a heat gun (Figure S1b). This is advantageous over a conventional hot plate or oven annealing, as the heat flows from the top which is less aggressive for the underlying layers and the substrate. This can be particularly important for the perovskite material, which has a relatively low thermal stability.[27] For the annealing optimization, the distance between the gun tip and the sample was kept at 5 cm, and the temperature of the heat gun was set to 200 °C. We monitored variations in the bulk resistance of the carbon layer as a function of annealing time. The initial drop in the bulk resistance we assign to the removal of solvent and binders present in the paste. We reached the bulk resistance of 55 Ω after 5 min of annealing in these conditions and calculated the sheet resistance to be around 10 $\Omega/\square$. The graph displaying optimization of the annealing time and images presenting the setup are shown in Figure S1c.

We blade-coated the optimized carbon layer as a back-contact electrode in a flexible planar heterojunction perovskite solar cell of p−i−n configuration. We used the following device structure: PET-IZO/poly(triarylamine) (PTAA)/$Cs_{0.04}(MA_{0.17}FA_{0.83})_{0.96}Pb(I_{0.83}Br_{0.17})_3$/[6,6]-phenyl-C61-butyric acid methyl ester (PCBM)/carbon. We applied the state-of-the-art perovskite composition, $Cs_{0.04}(MA_{0.17}FA_{0.83})_{0.96}Pb(I_{0.83}Br_{0.17})_3$, which was processed by spin-coating on top of PTAA with a solvent engineering method.[28] We carried out all the device processing using a flexible PET foil as a substrate. The cross-section FIB-SEM (focused ion beam scanning electron microscopy) image of the described layer stack is shown in Figure S2a. We observed that large carbon flakes present in the formulation paste (sizes reaching 5−10 μm) can penetrate through the soft, organic layers and lead to a significant drop of shunt resistance. The example of the current density−voltage (JV) characteristics of one of the shunted devices is shown in Figure S2b. The device exhibits a large injection current at a low voltage bias, i.e., very low shunt resistance. The mechanical damage can be particularly severe when the screen-printing method is used for carbon deposition, as this technique exerts substantial pressure on the substrate being coated during the process.

In order to mitigate the mechanical damage, we tested different buffer layers, which when deposited on the surface of the device stack could act as a mechanical shield, protecting the underlying layers from carbon damage. For that purpose, we tried metal oxides deposited by atomic layer deposition (ALD) (SnO_2 and Al_2O_3), solution-processed metal oxide nanoparticles (NPs) (SnO_2 and ZnO), and thermally evaporated chromium. Cross-section FIB-SEM images (Figure S3) of the structures with different buffer layers indicate that some of these materials indeed can safeguard the perovskite stack.
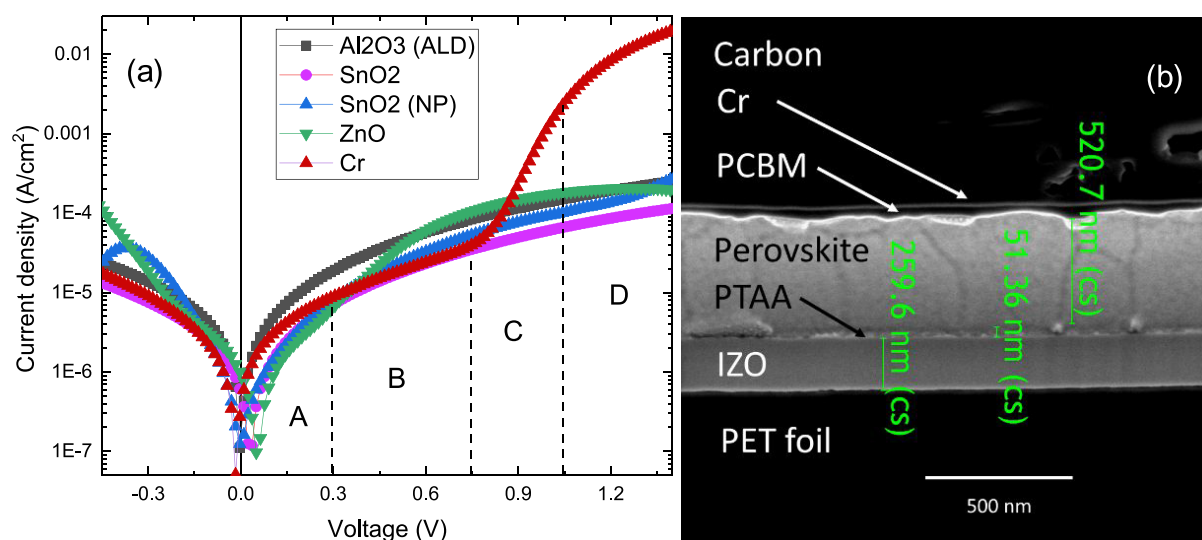
Figure 1. (a) Dark JV curves of flexible p−i−n perovskite solar cells with different buffer layers and a carbon back-contact electrode, marked A−D. The regions are mainly determined by a shunt current, recombination current in a diode space-charge region, diffusion current, and diffusion current limited by a series resistance, respectively. (b) Cross-section FIB-SEM image of a PSC with Cr used as a buffer layer and carbon electrode.

Then, we measured dark JV curves of the solar cells with different buffer layers to probe the current flow ability (Figure 1a). In the graph, we marked four different regions, A, B, C, and D, which correspond to the shunt current region, recombination current in a diode space-charge region, diffusion current, and diffusion current limited by a series resistance, respectively.[29] We observe that the cells with different metal oxides display a very low diffusion current (region C and D), pointing at the insulating character of the interface with these buffer layers. Interestingly, the solar cell with a Cr interlayer exhibits no significant leakage current (high enough shunt resistance) and no significant series resistance, which could impede the current flow. This suggests that the evaporated Cr thin film, thanks to its high ductility, could provide good mechanical protection for the perovskite device stack during carbon processing. Additionally, it facilitates electron transfer between PCBM and carbon. We are showing the cross-section microscope image of this device structure in Figure 1b. The SEM image shows carbon flakes very well separated from the perovskite device stack with an ultrathin Cr layer, proving its shielding effect. The evaporated film was 5 nm thick, and the carbon of 20 μm was processed according to the optimized conditions described above. A photo of such a perovskite solar cell with the Cr/C back-contact, processed on a flexible substrate, is shown in Figure S4. After the Cr thermal evaporation process, the cells were exposed to air before carbon printing. This could lead to partial chromium oxidation and formation of a dense bilayer structure of Cr/Cr$_2$O$_3$, as demonstrated previously by Kaltenbrunner et al.[30]

In the next step, we tested the photovoltaic performance of fabricated flexible p−i−n perovskite solar cells with the Cr/C back-contact electrode and compared it with the reference cells utilizing an evaporated Cr/Ag (100 nm) electrode. Schematic structures of such devices are shown in Figure 2a,b. Figure 2c shows the JV characteristics of the champion devices with an active area of 1 cm^2 under AM 1.5G illumination (100 mW/cm^2). We present two scan directions, forward bias (FB) to short circuit (SC) and short circuit (SC) to forward bias (FB). All the cells display very small hysteretic behavior. The best cell with the Cr/C yields the efficiency of 15.18% (RS), with V_{OC}

of 1.05 V, J_{SC} of 20.93 mA/cm^2, and FF of 68.97%. This is very similar to the best reference device (Cr/Ag) performance, which features the PCE of 15.71%, V_{OC} of 1.01 V, J_{SC} of 20.13 mA/cm^2, and 77.09% FF. All the photovoltaic parameters extracted from the JV curves are listed in Table 1.

The reduction in FF in the carbon device could be explained by the limitations in carrier transport through the carbon layer (sheet resistance above 10 $\Omega/\square$) when compared to the silver layer (sheet resistance below 2 $\Omega/\square$). Additionally, the contribution of series resistance can be more pronounced in devices with larger active areas, such as 1 cm^2 we used here. Galagan et al. demonstrated a 7% drop in FF when the cell width was increased from 0.5 to 1 cm for a 10 $\Omega/\square$ transparent electrode.[31] Therefore, it is important to optimize the cell dimensions for reducing the FF drop. Nevertheless, we observed a small increase in voltage and current densities for the champion Cr/C devices.

To corroborate the performance derived from the JV characterization, we present a stabilized power output (SPO) close to the maximum power point, which reflects the true sustainable power conversion efficiency of the solar cell. In Figure 2d, we can observe a stable SPO for over 30 s exhibited by both of the device types. We also measured the external quantum efficiency (EQE) of these cells; the spectra are shown in Figure 2e. The shape with an onset at 780 nm is the same for the reference and carbon-based device. We extracted the bandgap value of 1.58 eV for the Cs$_{0.04}$(MA$_{0.17}$FA$_{0.83}$)$_{0.96}$Pb-(I$_{0.83}$Br$_{0.17}$)$_3$ perovskite. We integrated the current density in a spectral range from 350 to 800 nm, obtaining 19.74 and 19.14 mA/cm^2 for the carbon and silver devices, respectively. The integrated values from EQE were comparable to the current densities obtained from the JV curves, 20.09 mA/cm^2 for the carbon cell and 19.33 mA/cm^2 for the silver cell. Photovoltaic parameters of a large set of samples (30 individual cells) are shown in Figure 2f and Figure S5. We obtained good reproducibility of photovoltaic parameters for these cells, with an average efficiency close to 13% for both carbon and silver contacts. Table S1 contains average values of all the photovoltaic parameters (PCE, J_{SC}, FF, V_{OC}).
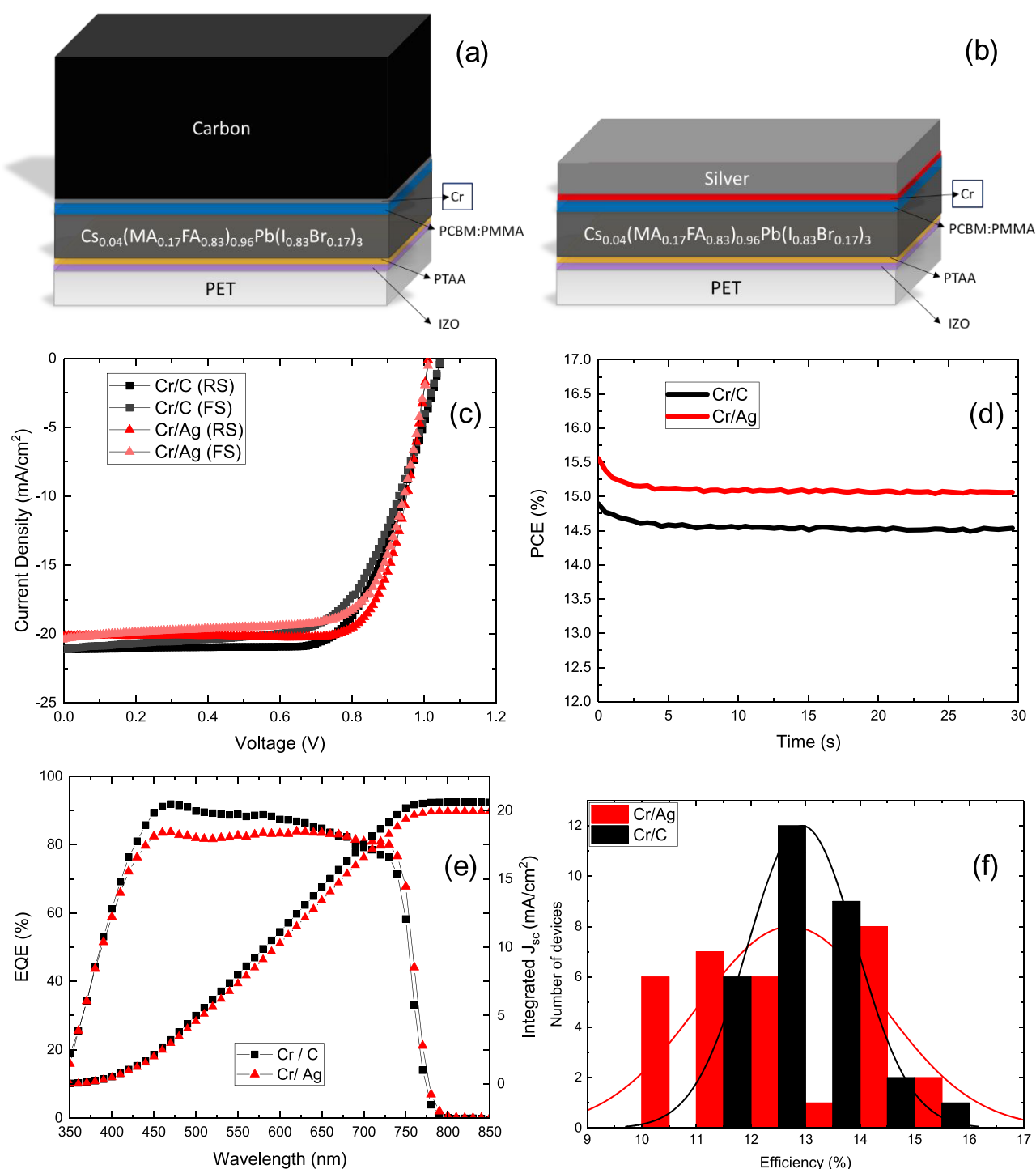
Figure 2. Schematics of p−i−n perovskite solar cell device structures, with (a) Cr/C and (b) Cr/Ag back-contact electrodes. (c) JV characteristics of the best devices (1 cm^2 area), fabricated on a flexible substrate, measured in reverse and forward scan directions. (d) Stabilized power output of the same cells monitored over 30 s. (e) EQE spectra and integrated current densities of the same cells, measured in a spectral range from 350 to 850 nm. (f) Histogram of 30 individual cells with Cr/C and Cr/Ag back-contacts.

Table 1. Photovoltaic Parameters of Cr/C and Cr/Ag Devices under Reverse (RS) and Forward (FS) Scan Directions

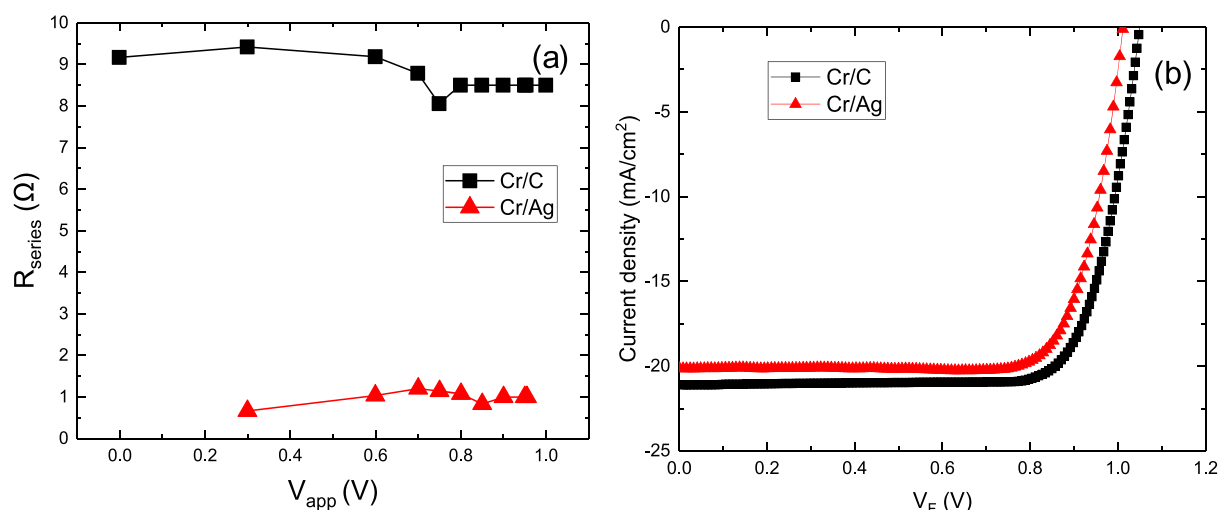| p−i−n		PCE[%]	J_{SC} [mA/cm^2]	FF [%]	V_{OC} [V]	integrated J_{SC} [mA/cm^2] (EQE)
Cr/carbon	RS	15.18	20.92	68.97	1.05	20.56
	FS	13.94	21.18	63.07	1.04	
Cr/silver	RS	15.71	20.13	77.09	1.01	19.94
	FS	14.63	20.34	71.05	1.01	

Figure 3. (a) R_{series} parameter derived from the impedance measurements at different applied voltages (V_{app}) of the Cr/C and Cr/Ag perovskite cells. (b) Calculated JV characteristics using the corrected voltage (V_F) with no series resistance contribution, corresponding to the Cr/C and Cr/Ag device types.

The Cr interlayer plays a crucial role in facilitating effective electron transfer to the back-contact material. To the best of our knowledge, this is the highest reported efficiency for the flexible PSC with a carbon electrode. Additionally, it is the first demonstration of the use of carbon electrode in the p−i−n cell configuration.

To compare the interface characteristics of the cells with the Cr/C and Cr/Ag back-contact variations, we carried out impedance spectroscopy measurements (EIS) of these devices, in the dark and under illumination conditions. This technique has been widely used as a powerful tool to study the electrochemical and solid-state devices in operational conditions. We performed the measurement by applying a sinusoidal voltage perturbation (V_{AC}) with different frequencies (ω) over a direct applied voltage (V_{app}) set to the sample and measured the AC current response (I_{AC}).[32] The impedance (Z) is calculated by eq 1:

$$Z(\omega) = \frac{V_{AC}}{I_{AC}} \tag{1}$$

For each V_{app}, we obtained a spectrum which was fitted with the equivalent circuit model. Figure S6a shows the impedance spectra of the Cr/C and Cr/Ag devices under illumination with the V_{app} close to V_{OC}. The proposed circuit model with the fitting parameters and their description is provided in Figure S6b. We found that the series resistance (R_{series}) was a key parameter to analyze the differences in the response of our devices. In Figure 3a, we show that the obtained R_{series} for the Cr/C devices was in the range 8−9 Ω, while that for Cr/Ag presented a value around 0.7 Ω.

We calculated the corrected voltage (V_F), corresponding to the removal of the effect of R_{series} in the device at each applied voltage, following the method reported by Fabregat-Santiago et al.[32] Then, we recalculated the parameters of the JV_F characteristics of the cells from Figure 2a (reverse scan), and present it in Figure 3b. This plot makes evident that the carbon-based device performance is limited by its high series resistance. From the comparison with the impedance response of the Cr/Ag device, we can conclude that the lower conductivity of the carbon layer is the main contributor to the R_{series}. The recalculated JV_F curves for both device types

show very similar FF values, 77.22% and 77.21%, for the Cr/C and Cr/Ag, respectively. The PCE of the Cr/C device without series resistance would increase from 15.18% to 17.14%. In Table S2, we show the corrected parameters for both cell types. We note that the higher J_{SC} obtained for the Cr/C sample in comparison with the Cr/Ag cell also contributes to the small improvement in V_{OC}. The analysis we provide here shows the potential of the p−i−n perovskite solar cell with the Cr/C back-contact electrode. The strategies to reduce the limiting series resistance can include increasing carbon paste conductivity or optimization of a device design to shorten the traveling path of charge carriers (smaller device width).[31]

We performed transient photocurrent (TPC) and transient photovoltage (TPV) measurements to further corroborate the analysis of interface characteristics with different back-contact electrode materials in the studied devices.[33,34] The TPC measurement was performed in a high perturbation regime, which means that the cell went from dark to a specific illumination set by an LED source. The cell was kept in the short-circuit condition during the entire measurement. The decay of current density was monitored over time after switching off the light. Figure S7 shows the transient decays for the Cr/C and Cr/Ag devices obtained with the perturbation light intensity corresponding to 1.5 suns. We integrated the current density time decay to obtain the extracted charge density. Figure 4a shows the charge density values derived at different perturbation light intensities (from 0.1 to 1.5 suns). From the plots, we can deduce that both of the back-contact types, Cr/Ag and Cr/C, exhibit very similar charge extraction properties. Interestingly, at higher light intensities, the Cr/C device shows even superior extraction efficacy than the reference Cr/Ag cell.

The TPV measurement was performed in a small perturbation regime. The cell was kept at open circuit, with a specific background illumination applied from the LED source. Then, a small overcurrent was sent to the LED to create a voltage perturbation (20 mV), with a decay that was subsequently monitored. In Figure 4b, we show the extracted recombination lifetimes derived from fitting voltage decay curves for different light intensities. Both solar cell types exhibit similar recombination dynamics at higher light
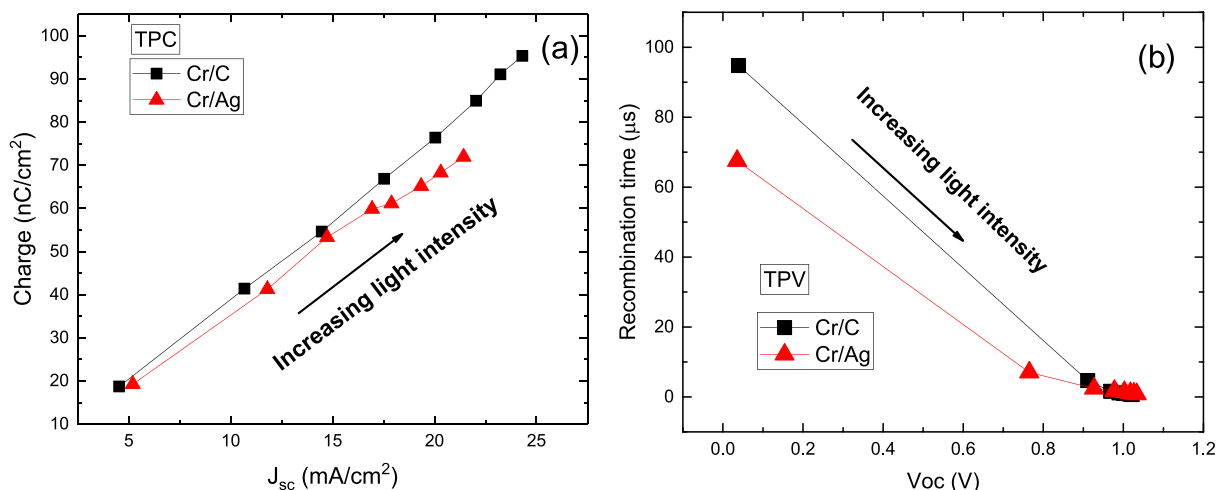
Figure 4. Analysis of TPC/TPV measurements of PSCs with the Cr/C and Cr/Ag back-contact electrodes: (a) charge density extracted from the photocurrent decay measurements, plotted as a function of a short-circuit current density corresponding to varied perturbation light intensities; (b) recombination lifetimes derived from the photovoltage decay fitting, plotted as a function of an open-circuit voltage at varied background light intensities.

intensities (inset in Figure 4b), while at low light bias the Cr/C device displays noticeably slower recombination, which corresponds to the longer carrier lifetimes.

So far, we have shown the effect of using an ultrathin Cr interlayer for enabling efficient electron extraction in the p−i−n carbon-based perovskite solar cells. To check the universality of this material, we also fabricated PSCs utilizing Cr as a back-contact buffer layer in an n−i−p cell configuration. We used the following device structure: PET-IZO/SnO$_2$/Cs$_{0.04}$(MA$_{0.17}$FA$_{0.83}$)$_{0.96}$Pb(I$_{0.83}$Br$_{0.17}$)$_3$/PTAA/Cr/carbon (device scheme is shown in Figure S8a). The cross-section FIB-SEM image documenting the 5 nm thick Cr interlayer between the PTAA hole transporter and the carbon electrode is shown in Figure S8c. Figure S8d displays the JV curves of the best devices (cell area of 1 cm^2, flexible substrate), with and without Cr. The champion Cr/C device featured a J_{SC} of 19.49 mA/cm^2, FF of 60.72%, and V_{OC} of 1.02 V, altogether resulting in the PCE of 12.06% when measured in the reverse scan direction. The reference carbon device without any buffer layer delivered the PCE of 10.68%, with J_{SC} of 19.44 mA/cm^2, FF of 55.64%, and V_{OC} of 0.99 V. All the perovskite parameters in both scan directions are shown in Table S3. We can observe negligible hysteresis in both device types. The use of a Cr interlayer resulted in an 8% increase of FF. Figure S9 shows the statistics of photovoltaic parameters (based on 10 individual cells). From these results, it is evident that Cr can effectively work in both cell configurations, facilitating either electron or hole transfer to the electrode.

As we discussed above, perovskite layers due to their ionic character are susceptible to electric field-driven movement of charged species and various redox reactions, including an oxidation of metallic back-contact material with halide ions. Many of these processes can lead to the rapid decrease of photovoltaic performance, which is further accelerated at elevated temperatures.[14] In order to analyze the long-term stability of our flexible perovskite solar cells with different back-contact materials, we carried out an aging test at the maximum power point, under constant illumination (LED source; intensity, 600 W/m^2), inside the nitrogen-filled glovebox at the temperature of 35−40 °C. Figure 5a displays the PCE, J_{SC}, FF, and V_{OC} evolution of p−i−n devices utilizing

different back-contact electrodes (Ag, Cr/Ag, and Cr/C), and an n−i−p device with the Cr/C electrode. Each data point was obtained by removing the cell from the glovebox and measuring JV characteristics at the solar simulator. The p−i−n device with the Ag electrode recorded a 20% drop of performance after 600 h of aging. From all the photovoltaic parameters, the short-circuit current density undergoes the largest decline. The p−i−n cell with the Cr interlayer shows significantly enhanced stability, which preserved over 90% of the initial performance after 1000 h. This suggests that the primary origin of the observed performance deterioration is caused by the reaction between halide ions and silver material, which leads to the silver halide formation and impedes the charge collection at the interface.[14] Chromium can provide an effective barrier for halide diffusion, suppressing this reaction.[30] The p−i−n device with the Cr/C contact shows a very stable performance with a negligible drop in efficiency over the studied time window. Interestingly, the n−i−p cell with the Cr/C contact exhibited a sizable increase in J_{SC} and FF, leading to the rise of PCE from 11.25% to 12.71% after 1000 h of aging. This effect can originate from the improved interface characteristics at the PTAA/Cr/C contact.

Furthermore, we studied a thermal stability of flexible perovskite solar cells with different electrodes. We kept the devices on a hot plate at 85 °C inside the glovebox and monitored the evolution of the solar cell performance over time. We show the changes in the PCE, J_{SC}, FF, and V_{OC} values for the Cr/C and Cr/Ag devices in Figure 5b, plotted over the period of 1000 h. We observe a remarkable thermal stability of the device with the Cr/C back-contact, showing a very small effective drop of performance in the studied time window. The cells with the Cr/Ag electrode deteriorated much faster, losing nearly 20% of the initial PCE after only 30 h. The drop of performance is primarily affected by the losses in current densities. Additionally, we noticed a clear visual change in the silver layer, from a shiny appearance before the test to a matte, darker look after the test (see Figure S10). Enhanced ionic mobility at higher temperatures seems to diminish the Cr barrier effect, which results in the degradation of the Ag layer and the drop in performance, whereas the Cr/C device remains unaffected. Overall, it is evident that the Cr/C layer
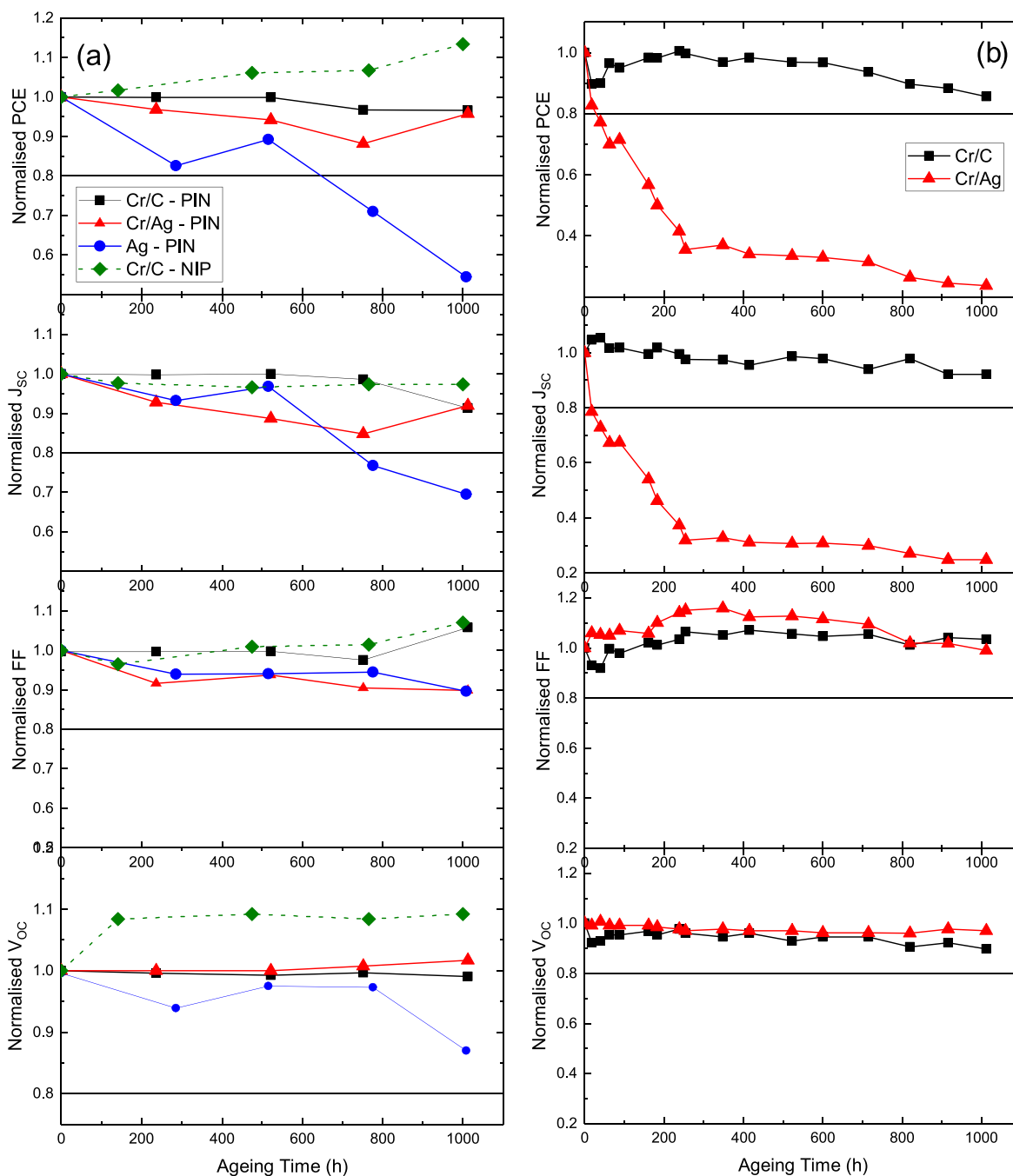
Figure 5. (a) Time evolution of normalized photovoltaic parameters (from the top: efficiency, short-circuit current density, fill factor, open-circuit voltage) of the perovskite solar cells of p−i−n and n−i−p architectures and different back-contact electrodes, kept at the maximum power point inside the nitrogen-filled glovebox (LED light source; intensity, 600 W/m²; temperature, 35−40 °C). (b) Evolution of normalized photovoltaic parameters of p−i−n devices with the Cr/C and Cr/Ag back-contact electrodes, aged inside the glovebox at 85 °C.

stack used as a back-contact electrode significantly enhances the stability of a p−i−n perovskite device structure.

In summary, we have demonstrated a solution-processed carbon layer as an effective back-contact material for the flexible p−i−n perovskite solar cells. By modifying the interface between the n-type collection layer and carbon with the carefully selected Cr buffer layer, we obtained an Ohmic contact with a good electron (and hole) extraction efficacy. Detailed analysis of the character of that interface has been provided with the impedance spectroscopy and transient photocurrent/photovoltage decay measurements. Additionally, the Cr interlayer preserves the solar stack from a mechanical

damage which can occur during the carbon processing. The best Cr/C device, fabricated on a PET foil with the large active area (1 cm²), reached 15.18% of power conversion efficiency. We have also shown the applicability of the Cr buffer layer in n−i−p PSC configuration, obtaining 12.06% efficiency for the flexible, large-area device with the Cr/C back-contact. Additionally, we are showing exceptional operational (maximum power point, 1000 h) and thermal (85 °C, 1000 h) stability of the flexible perovskite solar cells with the Cr/C back-contact, with minimal losses in the studied time window.

This work reveals that the carbon-based film can be used as the back-contact electrode in highly efficient perovskite solar

cells. Few considerations should to be taken into account to maximize the achievable power output, including the electronic contact at the interface with the carbon layer and its series resistance. Both factors should be well-balanced to avoid limitations to the optimal solar cell operation. The development of the solution-processable buffer layer, which would exhibit similar functionality to the Cr interlayer, provides an interesting outlook for future work. Highly conductive, two-dimensional materials (graphene, MXenes) constitute an attractive group of compounds to be considered for such purpose.

■ ASSOCIATED CONTENT

ⓢ Supporting Information

The Supporting Information is available free of charge at https://pubs.acs.org/doi/10.1021/acsaem.0c00702.

Full experimental methods and additional information and results (PDF)

■ AUTHOR INFORMATION

Corresponding Author

Konrad Wojciechowski − *Saule Technologies, Wroclaw PL 54-427, Poland; Saule Research Institute, Wroclaw PL 54-427, Poland;* ⓞ orcid.org/0000-0002-7664-801X; Email: konrad.wojciechowski@sauletech.com

Authors

Vivek Babu − *Saule Technologies, Wroclaw PL 54-427, Poland; CHOSE, Centre for Hybrid and Organic Solar Energy, Department of Electronics Engineering, University of Rome "Tor Vergata", Roma IT 00177, Italy;* ⓞ orcid.org/0000-0002-7579-754X

Rosinda Fuentes Pineda − *Saule Technologies, Wroclaw PL 54-427, Poland;* ⓞ orcid.org/0000-0003-2587-8795

Taimoor Ahmad − *Saule Technologies, Wroclaw PL 54-427, Poland; CHOSE, Centre for Hybrid and Organic Solar Energy, Department of Electronics Engineering, University of Rome "Tor Vergata", Roma IT 00177, Italy;* ⓞ orcid.org/0000-0001-9922-9603

Agustin O. Alvarez − *Institute of Advanced Materials, University Jaume I, Castello ES 12006, Spain;* ⓞ orcid.org/0000-0002-0920-5390

Luigi Angelo Castriotta − *CHOSE, Centre for Hybrid and Organic Solar Energy, Department of Electronics Engineering, University of Rome "Tor Vergata", Roma IT 00177, Italy;* ⓞ orcid.org/0000-0003-2525-8852

Aldo Di Carlo − *CHOSE, Centre for Hybrid and Organic Solar Energy, Department of Electronics Engineering, University of Rome "Tor Vergata", Roma IT 00177, Italy;* ⓞ orcid.org/0000-0001-6828-2380

Francisco Fabregat-Santiago − *Institute of Advanced Materials, University Jaume I, Castello ES 12006, Spain;* ⓞ orcid.org/0000-0002-7503-1245

Complete contact information is available at:
https://pubs.acs.org/10.1021/acsaem.0c00702

Notes
The authors declare no competing financial interest.

■ ACKNOWLEDGMENTS

■ REFERENCES

(1) Roy, P.; Kumar Sinha, N.; Tiwari, S.; Khare, A. A Review on Perovskite Solar Cells: Evolution of Architecture, Fabrication Techniques, Commercialization Issues and Status. *Sol. Energy* **2020**, *198*, 665−688.

(2) Cell Efficiency Chart. https://www.nrel.gov/pv/cell-efficiency.html (accessed: January 2020).

(3) Akin, S.; Arora, N.; Zakeeruddin, S. M.; Grätzel, M.; Friend, R. H.; Dar, M. I. New Strategies for Defect Passivation in High-Efficiency Perovskite Solar Cells. *Adv. Energy Mater.* **2020**, *10*, 1903090.

(4) Dong, Q.; Fang, Y.; Shao, Y.; Mulligan, P.; Qiu, J.; Cao, L.; Huang, J. Electron-Hole Diffusion Lengths Larger 175 Mm in Solution-Grown CH3NH3PbI3 Single Crystals. *Science* **2015**, *347*, 967−970.

(5) Wehrenfennig, C.; Eperon, G. E.; Johnston, M. B.; Snaith, H. J.; Herz, L. M. High Charge Carrier Mobilities and Lifetimes in Organolead Trihalide Perovskites. *Adv. Mater.* **2014**, *26*, 1584−1589.

(6) Green, M. A.; Ho-Baillie, A.; Snaith, H. J. The Emergence of Perovskite Solar Cells. *Nat. Photonics* **2014**, *8*, 506−514.

(7) Amgar, D.; Aharon, S.; Etgar, L. Inorganic and Hybrid Organo-Metal Perovskite Nanostructures: Synthesis, Properties, and Applications. *Adv. Funct. Mater.* **2016**, *26*, 8576−8593.

(8) Wojciechowski, K.; Forgács, D.; Rivera, T. Industrial Opportunities and Challenges for Perovskite Photovoltaic Technology. *Sol. RRL* **2019**, *3*, 1900144.

(9) Huang, F.; Li, M.; Siffalovic, P.; Cao, G.; Tian, J. From Scalable Solution Fabrication of Perovskite Films towards Commercialization of Solar Cells. *Energy Environ. Sci.* **2019**, *12*, 518−549.

(10) Wang, R.; Mujahid, M.; Duan, Y.; Wang, Z. K.; Xue, J.; Yang, Y. A Review of Perovskites Solar Cell Stability. *Adv. Funct. Mater.* **2019**, *29*, 1808843.

(11) Khenkin, M. V.; Katz, E. A.; Abate, A.; Bardizza, G.; Berry, J. J.; Brabec, C.; Brunetti, F.; Bulović, V.; Burlingame, Q.; Di Carlo, A.; Cheacharoen, R.; Cheng, Y.-B.; Colsmann, A.; Cros, S.; Domanski, K.; Dusza, M.; Fell, C. J.; Forrest, S. R.; Galagan, Y.; Di Girolamo, D.; Grätzel, M.; Hagfeldt, A.; von Hauff, E.; Hoppe, H.; Kettle, J.; Köbler, H.; Leite, M. S.; Liu, S.; Loo, Y.-L.; Luther, J. M.; Ma, C.-Q.; Madsen, M.; Manceau, M.; Matheron, M.; McGehee, M.; Meitzner, R.; Nazeeruddin, M. K.; Nogueira, A. F.; Odabaşı, Ç.; Osherov, A.; Park, N.-G.; Reese, M. O.; De Rossi, F.; Saliba, M.; Schubert, U. S.; Snaith, H. J.; Stranks, S. D.; Tress, W.; Troshin, P. A.; Turkovic, V.; Veenstra, S.; Visoly-Fisher, I.; Walsh, A.; Watson, T.; Xie, H.; Yıldırım, R.; Zakeeruddin, S. M.; Zhu, K.; Lira-Cantu, M. Consensus Statement for Stability Assessment and Reporting for Perovskite Photovoltaics Based on ISOS Procedures. *Nat. Energy* **2020**, *5*, 35−49.

(12) Domanski, K.; Correa-Baena, J. P.; Mine, N.; Nazeeruddin, M. K.; Abate, A.; Saliba, M.; Tress, W.; Hagfeldt, A.; Grätzel, M. Not All That Glitters Is Gold: Metal-Migration-Induced Degradation in Perovskite Solar Cells. *ACS Nano* **2016**, *10*, 6306−6314.

(13) Li, J.; Dong, Q.; Li, N.; Wang, L. Direct Evidence of Ion Diffusion for the Silver-Electrode-Induced Thermal Degradation of Inverted Perovskite Solar Cells. *Adv. Energy Mater.* **2017**, *7*, 1602922.

(14) Svanström, S.; Jacobsson, T. J.; Boschloo, G.; Johansson, E. M. J.; Rensmo, H.; Cappel, U. B. The Degradation Mechanism of Silver Metal Deposited on Lead Halide Perovskites The Degradation Mechanism of Silver Metal Deposited on Lead Halide Perovskites. *ACS Appl. Mater. Interfaces* **2020**, *12*, 7212−7221.

(15) Hadadian, M.; Smått, J.-H.; Correa-Baena, J.-P. The Role of Carbon-Based Materials in Enhancing the Stability of Perovskite Solar Cells. *Energy Environ. Sci.* **2020**, *13*, 1377−1407.

(16) Meng, F.; Liu, A.; Gao, L.; Cao, J.; Yan, Y.; Wang, N.; Fan, M.; Wei, G.; Ma, T. Current Progress in Interfacial Engineering of Carbon-Based Perovskite Solar Cells. *J. Mater. Chem. A* **2019**, *7*, 8690−8699.

(17) He, R.; Huang, X.; Chee, M.; Hao, F.; Dong, P. Carbon-based Perovskite Solar Cells: From Single-junction to Modules. *Carbon Energy* **2019**, *1*, 109−123.

(18) Fagiolari, L.; Bella, F. Carbon-Based Materials for Stable, Cheaper and Large-Scale Processable Perovskite Solar Cells. *Energy Environ. Sci.* **2019**, *12*, 3437−3472.

(19) Ku, Z.; Rong, Y.; Xu, M.; Liu, T.; Han, H. Full Printable Processed Mesoscopic CH3 NH3 PbI 3 /TiO2 Heterojunction Solar Cells with Carbon Counter Electrode. *Sci. Rep.* **2013**, *3*, 3132.

(20) Grancini, G.; Roldán-Carmona, C.; Zimmermann, I.; Mosconi, E.; Lee, X.; Martineau, D.; Narbey, S.; Oswald, F.; De Angelis, F.; Graetzel, M.; Nazeeruddin, M. K. One-Year Stable Perovskite Solar Cells by 2D/3D Interface Engineering. *Nat. Commun.* **2017**, *8*, 15684.

(21) Zhou, H.; Shi, Y.; Wang, K.; Dong, Q.; Bai, X.; Xing, Y.; Du, Y.; Ma, T. Low-Temperature Processed and Carbon-Based ZnO/CH3NH3PbI3/C Planar Heterojunction Perovskite Solar Cells. *J. Phys. Chem. C* **2015**, *119*, 4600−4605.

(22) Chu, Q. Q.; Ding, B.; Peng, J.; Shen, H.; Li, X.; Liu, Y.; Li, C. X.; Li, C. J.; Yang, G. J.; White, T. P.; Catchpole, K. R. Highly Stable Carbon-Based Perovskite Solar Cell with a Record Efficiency of over 18% via Hole Transport Engineering. *J. Mater. Sci. Technol.* **2019**, *35*, 987−993.

(23) Liu, T.; Chen, K.; Hu, Q.; Zhu, R.; Gong, Q. Inverted Perovskite Solar Cells: Progresses and Perspectives. *Adv. Energy Mater.* **2016**, *6*, 1600457.

(24) Magomedov, A.; Al-Ashouri, A.; Kasparavičius, E.; Strazdaite, S.; Niaura, G.; Jošt, M.; Malinauskas, T.; Albrecht, S.; Getautis, V. Self-Assembled Hole Transporting Monolayer for Highly Efficient Perovskite Solar Cells. *Adv. Energy Mater.* **2018**, *8*, 1801892.

(25) Zheng, X.; Hou, Y.; Bao, C.; Yin, J.; Yuan, F.; Huang, Z.; Song, K.; Liu, J.; Troughton, J.; Gasparini, N.; Zhou, C.; Lin, Y.; Xue, D. J.; Chen, B.; Johnston, A. K.; Wei, N.; Hedhili, M. N.; Wei, M.; Alsalloum, A. Y.; Maity, P.; Turedi, B.; Yang, C.; Baran, D.; Anthopoulos, T. D.; Han, Y.; Lu, Z. H.; Mohammed, O. F.; Gao, F.; Sargent, E. H.; Bakr, O. M. Managing Grains and Interfaces via Ligand Anchoring Enables 22.3%-Efficiency Inverted Perovskite Solar Cells. *Nat. Energy* **2020**, *5*, 131−140.

(26) Deng, Y.; van Brackle, C. H.; Dai, X.; Zhao, J.; Chen, B.; Huang, J. Tailoring Solvent Coordination for High-Speed, Room-Temperature Blading of Perovskite Photovoltaic Films. *Sci. Adv.* **2019**, *5*, eaax7537.

(27) Zhao, X.; Park, N. G. Stability Issues on Perovskite Solar Cells. *Photonics* **2015**, *2*, 1139−1151.

(28) Saliba, M.; Correa-Baena, J. P.; Wolff, C. M.; Stolterfoht, M.; Phung, N.; Albrecht, S.; Neher, D.; Abate, A. How to Make over 20% Efficient Perovskite Solar Cells in Regular (n-i-p) and Inverted (p-i-n) Architectures. *Chem. Mater.* **2018**, *30*, 4193−4201.

(29) Liao, P.; Zhao, X.; Li, G.; Shen, Y.; Wang, M. A New Method for Fitting Current−Voltage Curves of Planar Heterojunction Perovskite Solar Cells. *Nano-Micro Lett.* **2018**, *10*, 1−8.

(30) Kaltenbrunner, M.; Adam, G.; Głowacki, E. D.; Drack, M.; Schwödiauer, R.; Leonat, L.; Apaydin, D. H.; Groiss, H.; Scharber, M. C.; White, M. S.; Sariciftci, N. S.; Bauer, S. Flexible High Power-per-Weight Perovskite Solar Cells with Chromium Oxide-Metal Contacts for Improved Stability in Air. *Nat. Mater.* **2015**, *14*, 1032−1039.

(31) Galagan, Y. Perovskite Solar Cells: Toward Industrial-Scale Methods. *J. Phys. Chem. Lett.* **2018**, *9*, 4326−4335.

(32) Fabregat-Santiago, F.; Bisquert, J.; Garcia-Belmonte, G.; Boschloo, G.; Hagfeldt, A. Influence of Electrolyte in Transport and Recombination in Dye-Sensitized Solar Cells Studied by Impedance Spectroscopy. *Sol. Energy Mater. Sol. Cells* **2005**, *87*, 117−131.

(33) Alsari, M.; Pearson, A. J.; Wang, J. T. W.; Wang, Z.; Montisci, A.; Greenham, N. C.; Snaith, H. J.; Lilliu, S.; Friend, R. H. Degradation Kinetics of Inverted Perovskite Solar Cells. *Sci. Rep.* **2018**, *8*, 6−11.

(34) Yaghoobi Nia, N.; Lamanna, E.; Zendehdel, M.; Palma, A. L.; Zurlo, F.; Castriotta, L. A.; Di Carlo, A. Doping Strategy for Efficient and Stable Triple Cation Hybrid Perovskite Solar Cells and Module Based on Poly(3-Hexylthiophene) Hole Transport Layer. *Small* **2019**, *15*, 1904399.